Wind-Induced Aerodynamic Effects on Multiple Side Setback Tall Buildings Using CFD Simulation

Amlan Kumar Bairagi and Sujit Kumar Dalui

Abstract The present study considers different types of setback tall building models and compares the aerodynamic study with the 1:1:2 regular-shape tall building model. The setback height is considered at $h/2$, and $2h/3$ levels from the base of the model. The setback distances are arranged on the single side, double side, and around the building at the considered $h/2$ and $2h/3$ levels. This study was conducted by Computational Fluid Dynamics (CFD) method. The drag and lift coefficients of the building due to wind load are correlated. Power spectral density (PSD) at the top and setback roofs are also compared. Finally, this study concludes that the model has setbacks around the building efficiently reducing 89% torsional moment compared to the regular square shaped model. The reduced frequency decrease on the setback model has a setback around it. Finally, this study suggests that setback distance and increase of setback number around the model can easily handle the wind velocity and control the torsional moment due to wind.

Keywords Computational fluid dynamics (CFD) · Power spectral density (PSD) · Dynamic analysis · Setback building · Wind load

1 Introduction

Wind load on tall buildings continuously challenges researchers for reliable design. Calculation of aerodynamic effects on irregular shaped tall buildings is difficult to compare to regular shaped tall building models. Several international codes have already guided the calculation procedure of wind load for conventional shape-building models and suggested wind tunnel studies for unconventional shaped building models. The analysis of wind load on wind tunnel testing is expensive and

A. K. Bairagi (✉) · S. K. Dalui
Department of Civil Engineering, Indian Institute of Engineering Science and Technology, Shibpur, Howrah, India
e-mail: amlan.bairagi.rs2016@civil.iiests.ac.in

S. K. Dalui
e-mail: sujit@civiil.iiests.ac.in

M. Nehdi et al. (eds.), *Proceedings of SECON'23*, Lecture Notes in Civil Engineering 381, https://doi.org/10.1007/978-3-031-39663-2_35

protracted. Therefore, researchers have considered Computational Fluid Dynamics (CFD) study to simulate the different aerodynamic effects on the prototype model. The irregular shape and asymmetric shape of the tall buildings are always conspicuous. But this type of irregularly shaped tall building aids to damage the structure due to wind load. Continuous change and modification of tall building shapes can control the wind effect. A large number of tall buildings have already introduced setbacks for the alluring architectural appearance. Kim et al. [1] considered various configurations such as corner modifications, taper, setback, openings, and twists tall building models for the aerodynamic and pedestrian level wind characteristics. Kim et al. [2] studied seventeen different types of super-tall building models such as basic and corner modification with corner cut, chamfered, oblique opening, tapered, inversely tapered, bulged, and helical with twist angles and observed the aerodynamic effects for the different wind angles. Wang and Zhang [3] noticed the crosswind displacement response of the chamfered tall building when the ratio is increased to 5% or the rounded ratio increased to 12.5%. Bairagi and Dalui [4] studied 48 setback tall building models and optimized them by genetic algorithm. Finally selected a single model which reduces 45–65% drag and 25–60% lift compared to the regular shape 1:1:2 square model. Several researchers already studied the 1:1:2 models in the wind tunnel [5, 6] and CFD [7–9] study. The present study considers 1:1:2 regular plan shaped tall buildings and six different types of setback tall buildings to compare the aerodynamic effects at the rooftop and setback roof of the buildings. Computational Fluid Dynamics (CFD) study has been employed for the study. The multiple levels and multiple setback models have drastically reduced the aerodynamic effect and the number of setbacks. Variation of setback distances can play an important role to cut back on the frequency of the structure.

2 Numerical Method

The present study considered the renormalization group (RNG) k-ε method for the simulation technique. The transport equation of the RNG k-ε model as shown in Eqs. (1–3) [8, 10]:

$$\frac{\partial}{\partial t}(k) + \frac{\partial}{\partial x_i}(\rho k u_i) = \frac{\partial}{\partial x_j}\left(\alpha_k \mu_{eff} \frac{\partial k}{\partial x_j}\right) + G_k + G_b - \rho\varepsilon - Y_M + S_k \tag{1}$$

$$\frac{\partial}{\partial t}(\rho\varepsilon) + \frac{\partial}{\partial x_i}(\rho\varepsilon u_i) = \frac{\partial}{\partial x_j}\left(\alpha_\varepsilon \mu_{eff} \frac{\partial \varepsilon}{\partial x_j}\right) + C_{1\varepsilon}\frac{\varepsilon}{k}(G_k + C_{3\varepsilon}G_b) - C_{2\varepsilon}\rho\frac{\varepsilon^2}{k} - R_\varepsilon + S_\varepsilon \tag{2}$$

where k is the turbulence kinetic energy, ε is the turbulent eddy dissipation, G_k is the generation of turbulence kinetic energy due to the mean velocity gradients, G_b is the generation of turbulence kinetic energy due to buoyancy, Y_M is the contribution of

the fluctuating dilatation in-compressible turbulence to the overall dissipation rate, $\alpha_{k,}$ and α_{ε} are the inverse effective Prandtl numbers for k and ε respectively, S_k and S_{ε} are user-defined source terms.

The scale elimination procedure in RNG theory results in a differential equation for turbulence viscosity:

$$d\left[\frac{\rho^2 k}{\sqrt{\varepsilon\mu}}\right] = 1.72\frac{\hat{v}}{\sqrt{\hat{v}^3 - 1 + C_v}}d\hat{v} \tag{3}$$

where, $\hat{v} = \frac{\mu_{eff}}{\mu}$, $C_v \approx 100$. For an accurate description of the variation of effective turbulence transport for effective Reynolds number, integrate $\mu_t = C\mu\rho k^2/\varepsilon$. For the high Reynolds number limit, the constant $C_\mu = 0.0845$ was used to calculate the turbulence viscosity (μ_t). The other constants used in RNG theory are $\sigma_\varepsilon = 0.719$, $C_{1\varepsilon} = 1.42$, $C_{2\varepsilon} = 1.68$.

3 Description of the Models

This study considers seven square plan shaped models. It initially considered a square plan shape tall building model (SQ) of length (l) = 250 mm, breadth (b) = 250 mm, and height (h) = 500 mm. Therefore, the l:b:h is 1:1:2. Similar type of six different setback tall building models are considered for the study. The models are considered setbacks at different levels and on different sides of the models. According to the setback location from the base of the model, the setback models are considered in two groups. The first group is considered a single setback and the second group is a double setback. The first group has three different models and setbacks at the h/2 level from the base. The second group of setback models has three different models at setback levels h/3 and 2h/3 from the base. At first, the study considered the single side single setback model ($SB1_a$) considered the setback at the h/2 level as shown in Fig. 1. The setback distance is considered at 0.2l distance from the edge. That is 20% of the length of the building. Similarly, model ($SB1_b$) has two setbacks at the h/2 level on the opposite side of the building. Here, the 20% setback distance is divided on the opposite side of the model. Therefore, the setback distance of the double-side single setback model is 0.1l. The $SB1_c$ model has a setback around the model at h/2 height. Therefore, the setback distance is 0.1l around the model. In this similar way, the $SB1_a$ model allowed for a single side double setback at level h/3 distance from the base and 2h/3 distance from the base. So, the 20% setback distance is equally divided at the different levels. Therefore, the setback distance of the single-side double setback model ($SB2_a$) is 0.1l. In this similar fashion, the $SB2_b$ and $SB2_c$ models have considered setback distance 0.1l at h/3 and 2h/3 levels. The setback distances are placed on the opposite side for the $SB2_b$ model and around the building for the $SB2_c$ model. The flow of 0° wind is considered along the y-axis and 90° wind along the x-axis.

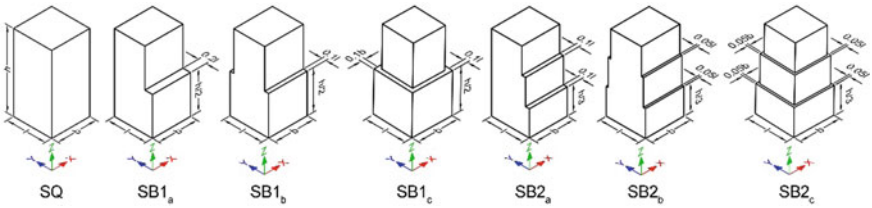

Fig. 1 Regular shape square building and different multiple-side setback building models

4 Domain and Meshing

The present study considered Computational Fluid Dynamics (CFD) method using ANSYS 2019 fluent package. The considered models are placed inside the domain for the analytical study. The inlet and both sidewalls are considered as 5*h* from the extreme edge of the model. The outlet of the model is placed at a 15*h* distance from the back side of the model for proper flow at the back side of the model. The top of the domain is placed at 6*h* from the base of the model as shown in Fig. 2a. The size of the domain is considered according to the guideline of the Architectural Institute of Japan (AIJ) [11]. This study considered 1:300 scale of the prototype model. The blockage ratio of the domain is 5%, which satisfies the AIJ guideline. The boundary conditions are selected as free-slip for the sidewalls of the domain and no-slip for the model walls. Tetrahedron meshing is considered around and inside the domain. The growth rate selected is 1.2 and the y^+ value is 3, which is less than 5 [12]. Mesh detail of the SQ model inside the domain is shown in Fig. 2b.

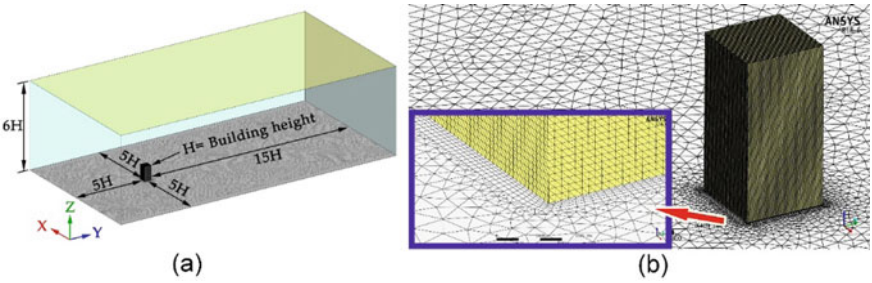

Fig. 2 **a** Dimension of the domain, **b** mesh diagram of SQ model inside the domain

5 Grid Sensitivity and Validation of the Study

This study considers the RNG k–ε turbulence model for the simulation purpose. The equation of fluctuation velocity (U), turbulence intensity (I), and turbulence energy (k) inside the domain are presented by Eqs. (4–6) [11].

$$U = U_h\left(\frac{Z}{Z_h}\right)^{\alpha} \tag{4}$$

$$I = \frac{u_u(z)}{U} = 0.1\left(\frac{Z}{Z_g}\right)^{(-\propto-0.005)} \tag{5}$$

$$k = \frac{u_u^2(z) + u_v^2(z) + u_w^2(z)}{2} \cong u_u^2(z) = (I \times U)^2 \tag{6}$$

where U_h is the boundary layer velocity, which was 10 m/s; $\alpha = 0.133$ is the power-law index for terrain category 2, Z_g is the boundary layer height determined by terrain category, u_u is the root-mean-square (RMS) value of velocity fluctuation in the streamwise direction. A similar type of experimental study of the same 1:1:2 building model was conducted by [4, 5, 13].

In Computational Fluid Dynamics (CFD) simulation, the grid sensitivity study is an important part [12]. In this study, the regular shaped square model was considered for the study. The SQ model was placed inside the domain and studied with tetrahedral meshing. A similar type of meshing has already been considered for past CFD studies and a good quality results have been found [14–16]. Coarse grid (Gr1), intermediate grid (Gr2), and fine grid (GR3) are used in this study. The node number and element numbers of the model and domain continuously increase with the increase of the number of edge divisions [17]. The pressure, force, and moment coefficient of the SQ model was simulated with the Gr1, Gr2, and Gr3 grid conditions and presented in Fig. 3a. Grid size-wise node numbers are considered to present the pressure (C_p), force (C_f), and moment (C_m) coefficients of the SQ model. Here, it is clear that the C_p, C_f, and C_m of the SQ model are continuously increasing with the increase in grid size [18]. Furthermore, this study compares the C_p and C_f of the SQ model for the adopted grid Gr3 with the pre-calculated values from the different international codes [19–22]. The pre-calculated values of C_p and C_f are adopted according to the considered aspect ratio (i.e., 1:1:2) of the SQ model. The simulated value of the SQ model has a good agreement with the considered international codes as shown in Fig. 3b. Therefore, this study adopted the Gr3 grid for further study of setback models.

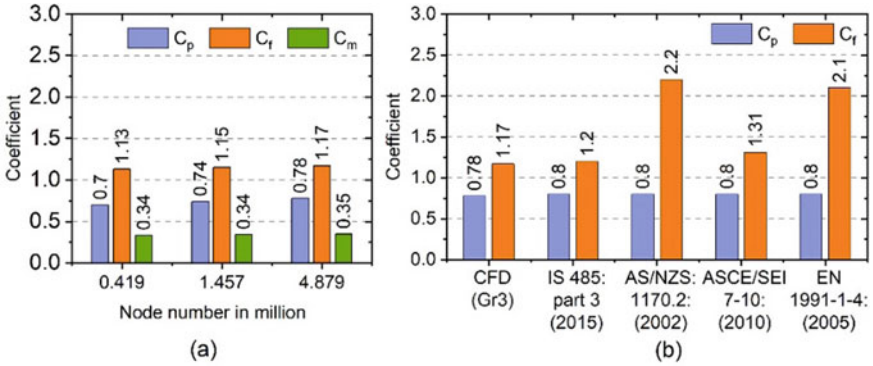

Fig. 3 **a** Grid sensitivity study of SQ model and **b** Comparative study of pressure and force coefficient between CFD and different international codes

6 Results and Discussions

6.1 Moment Coefficient Calculation

The models are experienced with the moment due to the flow of wind along the x and y axes. Simultaneously, the torsional moment about the z-axis is also calculated for the 0° and 90° wind angles. Moments about the x and y axes are represented as C_{mx} and C_{my}. The torsional coefficient is considered about the z-axis and represented as C_{mz}. The moment coefficients are calculated as [7]:

$$C_{mx} = \frac{F_x}{0.5\rho U_h^2 . A_x} = \frac{\sum_i C_p A_j \sin \propto_j}{\sum_i A_j \sin \propto_j} \tag{7}$$

$$C_{my} = \frac{F_y}{0.5\rho U_h^2 . A_y} = \frac{\sum_i C_p A_j \cos \propto_j}{\sum_i A_j \cos \propto_j} \tag{8}$$

$$C_{mz} = \frac{F_z}{0.5\rho U_h^2 . A_z} = \frac{\sum_i C_p A_j \cos \propto_j}{\sum_i A_j \cos \propto_j} \tag{9}$$

$$C_m = \sqrt{C_{mx}^2 + C_{my}^2} \tag{10}$$

where A_j is the supplementary area of point *j; sinα* and *cosα* are the direction vector of the point *j* along the x, y, and z axes. C_p is the pressure coefficient and C_m represents the global moment coefficient of the building. The global moment coefficient *(C_m)* of the buildings is calculated on the x and y axes for the 0° and 90° wind angles. Maximum values of torsional coefficients ($C_{mz,\max}$) are considered between 0° and 90° wind angles as shown in Fig. 4.

The fluctuation of the global moment coefficient (C_m) and torsional moment coefficient ($C_{mz,\max}$) are compared according to the initial SQ building model. Here, the

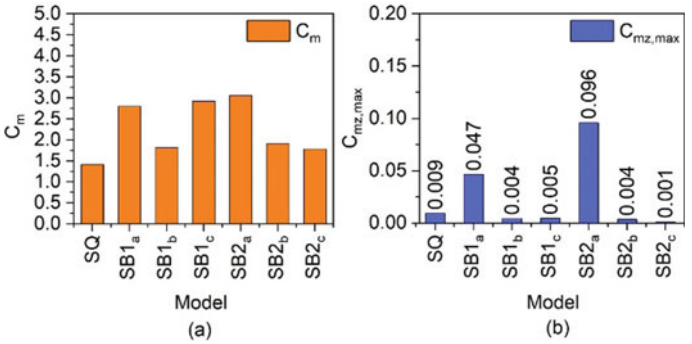

Fig. 4 Comparison of **a** global moment coefficient (C_m) and **b** maximum torsional moment coefficient ($C_{mz,\max}$) between the square and setback building models

study considers the C_m of the SQ model as the datum to compare the other considered models. A comparison of the percentage increase of the global moment and torsional moment coefficient is shown in Table 1. Upward (↑) and downward (↓) arrow marks behind the percentage data of Table 1 are represented the increase and decrease of C_m and $C_{mz,\max}$ of the respective model compared with the initial SQ model. As the SQ model is considered a datum of the comparative study, the comparative value of the SQ model in Table 1 is 0%. The model $SB2_c$ represented the minimum (20.58%) global moment coefficient compared to other setback models. Whereas, the $SB2_a$ model is experienced with maximum (53.65%) global moment coefficient. In this similar fashion, the torsional moment coefficient of setback buildings is compared with the SQ model. Here an interesting point is noticed. The $SB2_c$ model experienced a minimum torsional moment coefficient (0.001), which is 89% less than the SQ model. This type of variation of the global moment and torsional moment of setback models happens due to the setback distance and setback location. The setback of the $SB2_c$ model is considered around the building at the $h/2$ level. Therefore, the wind flows around it for 0° and 90° are similar. The $SB2_a$ has a double setback on a single side. According to the geometry of the model, the wind flow variation for 0° and 90° wind is different. Due to this reason, the $SB2_a$ model experienced the maximum torsional moment coefficient.

6.2 *Normalized Velocity Spectra*

The energy spectra of velocity or power spectral density (PSD) $Su(f)/\sigma 2$, (u = oscillating signal at the measuring point, f = frequency in Hz, σ = standard deviation of energy variation) was compared to the setback roof and top roof of the models. Another non-dimensional part Strouhal number ($S_u = fb/u$) was introduced here to evaluate the location of the peak of the dimensionless energy. One interested can follow the previous study [7, 23] for a detailed derivation of PSD and Strouhal

Table 1 Comparison of percentage increase of global moment coefficient (C_m) and torsional moment coefficient ($C_{mz,\max}$) according to the SQ model

Model	Increase of global moment (C_m) compared with SQ mode	Increase/decrease of the torsional moment ($C_{mz,\max}$) compared with SQ mode
SQ	0%	0%
SB1a	49.43% (↑)	80.85% (↑)
SB1b	22.03% (↑)	44.45% (↓)
SB1c	51.57% (↑)	55.56% (↓)
SB2a	53.65% (↑)	90.63% (↑)
SB2b	26.02% (↑)	44.45% (↓)
SB2c	20.58% (↑)	88.89% (↓)

number. The points are considered adjacent to the leeward face of the modes to observe the response of the spectral density [24]. Tapping points are considered at the edge of the rooftop for all the models. Another tapping point is fixed at the setback roof of double setback building models ($SB1_a$, $SB2_b$, and $SB2_c$). The tapping point locations that are demarcated are R1 and R2 for the first and second setback roof. According to the different shapes of the models, this study preferred normalized spectral density for 0° and 90° wind flow as shown in Figs. 5 and 6.

Variations of normalized velocity spectra for 0° wind angle at the rooftop of the SQ and Setback models are shown in Fig. 5a. The SQ model reflects the low-velocity spectral variation at the roof compared to the other setback models. The normalized PSD at the first setback region of the $SB1_a$ model represented the low variation due to its maximum setback distance as shown in Fig. 5b. Whereas Fig. 5c–d represented the normalized PSD of velocity at the first and second setbacks of the $SB2_a$, $SB2_b$, and $SB2_c$ models. Here $SB2_c$ model is reflected a lower value compared to the SB_{2b} and SB_{2c}. This type of variation is due to the setback distance ($0.1l$) of the $SB2_a$ model. Whereas, the other two models ($SB2_b$ and $SB2_c$) have a setback distance of $0.05l$. On the other hand, the normalized PSD of velocity is less at both setbacks of the $SB2_c$ model. This model produces low frequency at the setback region due to the proper distribution of setbacks around the model.

For the 90° wind angle, no such alteration of normalized PSD of velocity at the rooftop was noticed on the setback buildings as shown in Fig. 6a. An interesting point was noticed in the $SB2_a$ and $SB2_c$ models for 90° wind flow conditions. The normalized PSD for the velocity at the first and second setback region of the $SB2_a$ and $SB2_c$ modes are just opposite to the 0° wind flow condition as shown in Fig. 6b–c. The frequency of the $SB2_c$ model decreases at both the setback roof portion due to the uniform distribution of setbacks around the $SB2_c$ model. The 90° wind flow attacks the flat face of the $SB2_a$ model. Therefore, the fluctuation of wind flows attacks the setback region of the considered tapping points adjacent to the leeward face. But the $SB2_c$ model has a setback face for 90° wind flow. Therefore, the fluctuation of flow decreases due to the setback in the windward direction. Finally, the study came to the conclusions that, the setback around the building model may take an important

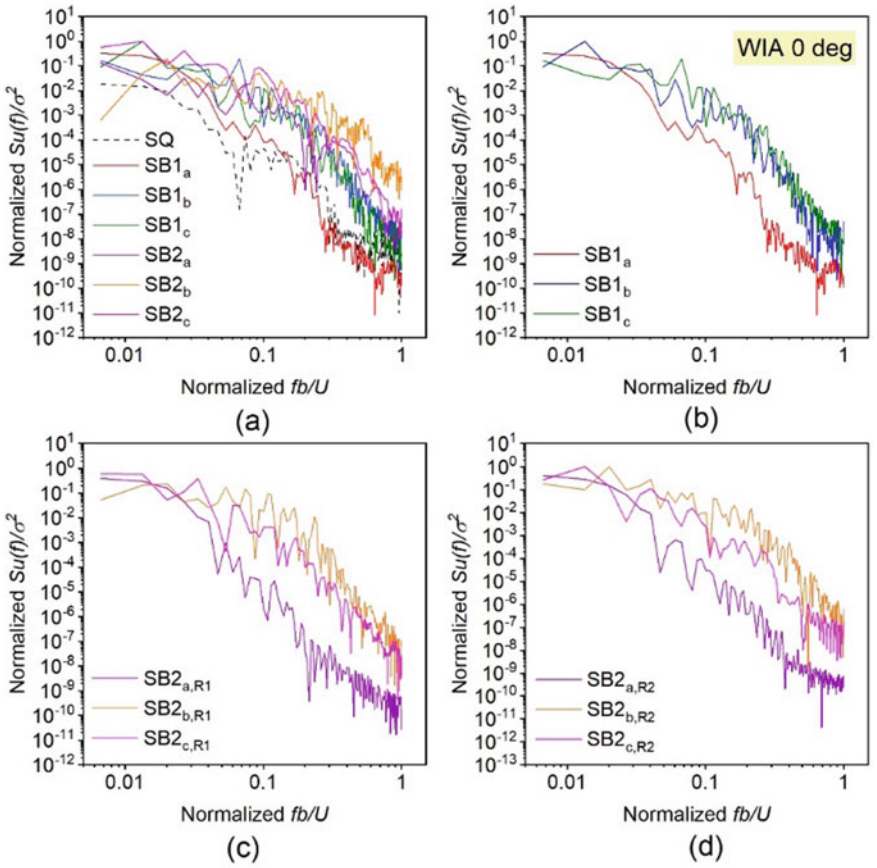

Fig. 5 Variation of the spectral density of velocity at the **a** top roof, **b** setback roof of single setback models, **c** setback roof (R1) of double setback model, **d** setback roof (R2) of double side setback model for 0° wind angle

role to reduce the aerodynamic effects on the setback buildings. Furthermore, the number of setbacks also plays an important part to reduce the frequency of velocity on the buildings.

7 Conclusions

This study focuses on the aerodynamic variation on the multiple numbers and multiple side setbacks of tall buildings and compared it with the regular square plan shape (1:1:2) building model. The study was conducted with the CFD simulation

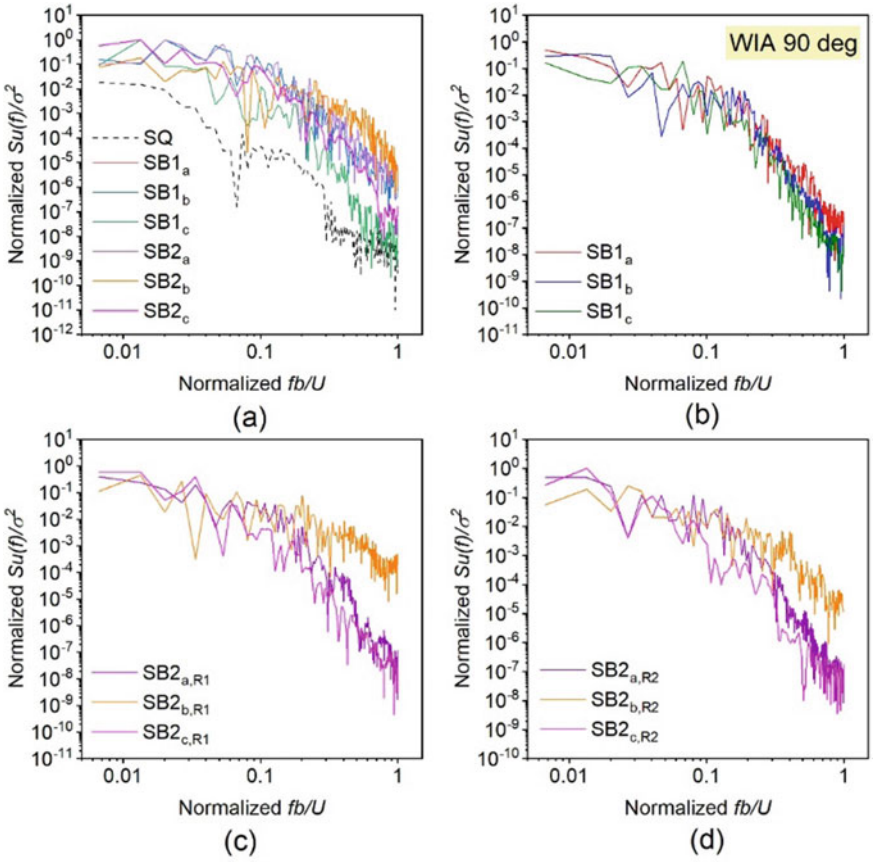

Fig. 6 Variation of the spectral density of velocity at the **a** top roof, **b** setback roof of single setback models, **c** setback roof (R1) of double setback model, **d** setback roof (R2) of double side setback model for 90° wind angle

along and across wind flow conditions. The following conclusions are established from the study.

1. The double setback building ($SB2_c$) model has setbacks around the model. This model experienced the same aerodynamic effects along and across wind conditions due to its geometry. Therefore, this model has a minimum torsional moment coefficient and is 89% less compared to the regular shape square (SQ) model.
2. The single-side double setback model (SB2a) efficiently reduces the frequency at the setback region for 0° wind flow, but it increases the frequency for the 90° wind angle due to the uniform windward face.
3. The $SB2_c$ model is very efficient to reduce the frequency of the velocity at the setback locations due to its uniform geometrical shape.

4. Finally, this study concluded the setback around the building model may take a foremost to reduce the aerodynamic effects on the setback buildings.
5. The number of setbacks also plays an important part to reduce the frequency of velocity on the building.
6. In this study, the conclusions are made according to the 1:1:2 (l:b:h) building models. Therefore, the results are suitable for the models have similar aspect ratio.
7. This study may further improve with the increase of setback distance and number. Also, it may be studied for different aspect ratios.

Acknowledgements The authors would like to express his gratitude to Sagata Jana, Assistant Teacher, at Ichapur Northland High School for her valuable guidance to modify the manuscript. The authors thank the editor for deciding on the manuscript in the reputed conference proceedings and book chapter. The authors also thank the reviewers for their valuable comments on the manuscript.

Funding The authors declare no specific funding for this work.

References

1. Kim YC, Xu X, Yang Q, Tamura Y (2019) Shape effects on aerodynamic and pedestrian-level wind characteristics and optimization for tall and super-tall building design. Int J High-Rise Build 8(4):235–253. https://doi.org/10.21022/IJHRB.2019.8.4.235
2. Kim W, Yoshida A, Tamura Y (2019) Wind-induced aerodynamic instability of super-tall buildings with various cross-sectional shapes. Int J High-Rise Build 8(4):303–311. https://doi.org/10.21022/IJHRB.2019.8.4.303
3. Wang L, Zhang W (2023) The influence of chamfered and rounded corners on vortex-induced vibration of super-tall buildings. Appl. Sci. 13
4. Bairagi AK, Dalui SK (2022) Minimization of wind load on setback tall building using multiobjective optimization procedure. Wind Struct Int J 35(3):157–175
5. Meng Y, Hibi K (1998) Turbulent measurements of the flow field around a high-rise building. J Wind Eng 76:55–64. https://doi.org/10.5359/jawe.1998.76_55
6. Kim YC, Kanda J, Tamura Y (2011) Wind-induced coupled motion of tall buildings with varying square plan with height. J Wind Eng Ind Aerodyn 99(5):638–650. https://doi.org/10.1016/j.jweia.2011.03.004
7. Bairagi AK, Dalui SK (2021) Prediction of pressure coefficient on setback building by artificial neural network. Can J Civ Eng. https://doi.org/10.1139/cjce-2020-0100
8. Bairagi AK, Dalui SK (2021) Wind environment around the setback building models. Build Simul 14(October):1525–1541. https://doi.org/10.1007/s12273-020-0758-3
9. Khaled MF, Aly AM, Elshaer A (2021) Computational efficiency of CFD modeling for building engineering: an empty domain study. J Build Eng 42(May):102792. https://doi.org/10.1016/j.jobe.2021.102792
10. Ansys 15 (2013) ANSYS fluent theory guide
11. Tominaga Y et al (2008) AIJ guidelines for practical applications of CFD to pedestrian wind environment around buildings. J Wind Eng Ind Aerodyn 96(10–11):1749–1761. https://doi.org/10.1016/j.jweia.2008.02.058
12. Franke J, Hellsten A, Schlünzen H, Carissimo B (2010) The best practise guideline for the CFD simulation of flows in the urban environment: an outcome of COST 732. In: The fifth international symposium on computational wind engineering, pp 1–10

13. Bairagi AK, Dalui SK (2020) Estimation of wind load on stepped tall building using CFD simulation. Iran J Sci Technol Trans Civ Eng. https://doi.org/10.1007/s40996-020-00535-1
14. Wijesooriya K, Mohotti D, Amin A, Chauhan K (2021) Comparison between an uncoupled one-way and two-way fluid structure interaction simulation on a super-tall slender structure. Eng Struct 229:111636. https://doi.org/10.1016/j.engstruct.2020.111636
15. Singh J, Roy AK (2019) Wind pressure coefficients on pyramidal roof of square plan low rise double storey building. Comput Eng Phys Model 2(1):1–16. https://doi.org/10.22115/cepm.2019.144599.1043
16. Weerasuriya AU, Zhang X, Lu B, Tse KT, Liu CH (2021) A Gaussian process-based emulator for modeling pedestrian-level wind field. Build Environ 188:107500. https://doi.org/10.1016/j.buildenv.2020.107500
17. Bairagi AK, Dalui SK (2018) Comparison of aerodynamic coefficients of setback tall buildings due to wind load. Asian J Civ Eng 19(2):205–221. https://doi.org/10.1007/s42107-018-0018-3
18. Bairagi AK, Dalui SK (2022) Prediction of pressure coefficient of setback building using backpropagation neural networks. Springer Singapore
19. IS 875 (part-3) (2015) Design loads (other than Earthquake) for buildings and structures-code of practice
20. AS/NZS 1170.2 (2011) Structural design actions—part 2: wind actions, vol 2
21. ASCE/SEI 7.10 (2010) Minimum design loads for buildings and other structures
22. EN 1991-1-4 (2005) Actions on structures—part 1–4: general actions—wind actions
23. Gavin HP (2016) Random processes, correlation, and power spectral density. Duke University, pp 1–28. https://doi.org/10.1007/978-1-4615-3406-8_43
24. Kim Y, Kanda J (2010) Characteristics of aerodynamic forces and pressures on square plan buildings with height variations. J Wind Eng Ind Aerodyn 98(8–9):449–465. https://doi.org/10.1016/j.jweia.2010.02.004